PROCEEDINGS, Thirty-Seventh Workshop on Geothermal Reservoir Engineering
Stanford University, Stanford, California, January 30 - February 1, 2012
SGP-TR-194

AN INVESTIGATION OF THE MICROSEISMIC EVENTS IN THE SALTON SEA GEOTHERMAL FIELD

Jingbo Wang[1], Dennise C. Templeton[1], David B. Harris[2]

1. Lawrence Livermore National Laboratory, 7000 East Ave, L -231, Livermore, CA, 94550, USA
2. Deschutes Signal Processing, LLC, P.O. Box 231, Maupin, OR, 97037, USA
e-mail: wang64@llnl.gov

ABSTRACT

We apply the empirical matched field processing (MFP) method to continuous seismic data to detect and locate more microearthquakes than can be detected using only conventional earthquake detection techniques. We demonstrate that empirical MFP can complement existing catalogs and techniques by increasing earthquake catalog completeness. The empirical MFP method finds events in the continuous data stream by identifying signals that match pre-defined master templates. We identify and construct representative master templates using the Southern California Earthquake Data Center (SCEDC) earthquake catalog and continuous waveform data of events originating within the Salton Sea Geothermal Field study area. We identify 231 master templates that have at least four good quality stations. We apply the empirical MFP method to continuous seismic data collected at the Salton Sea Geothermal Field between November 2009 and December 2010. The MFP method successfully identified 6496 local events, while the original catalog only reported 1536 events. We use subsets of the data to investigate the optimal frequency band in which to perform the matching operation and to perform a Coulomb stress change study. Our Coulomb stress modeling, using 21 fault mechanism solutions, shows the correlation between the positive Coulomb stress region and the majority of the microseismicity. In addition, we investigate the lower event detection magnitude threshold of our network using the MFP method. It clearly shows the event detection threshold is extended to include many smaller earthquakes with magnitudes between 0 and 1. Therefore, we believe that the empirical MFP method, when combined with conventional methods, significantly improves network detection capabilities.

INTRODUCTION

Accurate identification and mapping of large numbers of microearthquakes is one technique that provides diagnostic information when determining the location, orientation and length of underground crack systems. Conventional earthquake location techniques are often employed to locate microearthquakes. These techniques require accurate picking of individual seismic phase onsets across a network of sensors and work best on seismic records containing a single well-recorded event with high signal-to-noise ratio. Seismic phase picking, however, can become difficult or impossible on seismic records containing large numbers of overlapping events or events with poor signal-to-noise ratios.

To aid in the seismic characterization of reservoir fracture networks, we complement traditional earthquake detection and location techniques with the empirical matched field processing (MFP) method. The empirical MFP method matches the spatial structure of incoming seismicity observed by a network of sensors to master templates keyed to potential event locations. Empirical MFP steers the array by summing signals observed over a network using complex phase and amplitude weights obtained from existing event templates [*Harris and Kvaerna, 2010*]. This is different from the conventional seismic array processing method, delay-and-sum beamforming, which steers an array by applying time delays to align waveforms recorded by array elements. Empirical MFP is different from traditional waveform correlation techniques because it decomposes the signal into many narrow frequency bands and treats each as independent quantities. This is done in order to suppress the dependence on source time function, which is inherent in traditional waveform correlation techniques.

Empirical MFP develops a catalog of matching templates from a collection of representative microearthquakes that densely sample the study volume. The earthquakes for the empirical master templates are initially located using conventional earthquake location techniques, and subsequently relocated using advanced processing techniques, however all future seismicity can be mapped using the computationally efficient MFP algorithm. In this paper, we apply this technique to continuous seismic

data, which includes two earthquake swarms, collected in the Salton Sea Geothermal Field between November 2009 and December 2010 to demonstrate the power of the detection capability of empirical MFP.

STUDY AREA

The Salton Sea geothermal field (SSGF) is located in Southern California at the southern end of the Salton Sea within the Salton Trough, an active tectonic pull-apart basin. A portion of the SSGF is situated within the Brawley Seismic Zone, which extends across the Salton Sea to connect with the San Andreas Fault to the north and the Imperial Fault to the south [*Fuis and Mooney, 1990*]. This zone is the most northerly of a series of spreading centers, distributed along the length of the Salton Trough and within the Gulf of California that can be associated with the East Pacific Rise. Rifting and intrusions produce high heat flow that metamorphoses the sedimentary rocks to shallow depths [*Fuis et al., 1984*].

A local surface seismic monitoring network, the EN network, monitors SSGF seismic activity. The EN network is composed of eight three-component seismic stations (Figure 1). The instruments are 4.5 Hz L15B three-component geophones. Since January 2008, continuous data from this network has been archived at the Southern California Earthquake Data Center (SCEDC). The data during this time period includes two of the largest seismic swarms that occurred in the SSGF since continuous seismic data has been archived at the SCEDC.

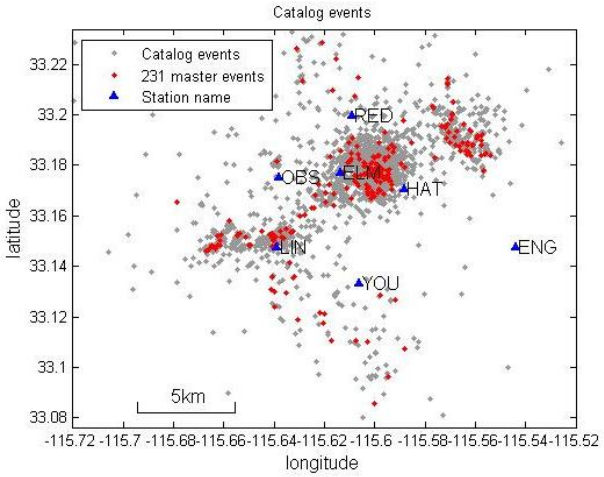

Figure 1. Map view of the seven seismic stations in the EN network which are included in this study. Seismic stations are indicated by blue triangles with station names. The grey dots are catalog events occurring between 2008 and 2010 [Haukson et al., 2012]. The master template events are marked in red.

METHOD

Our MFP technique is an adaptation of a signal processing technique originally developed to locate continuous underwater acoustic sources [*Bucker 1976; Baggeroer et al. 1993*]. We calculate the wavefield structure across an array by estimating the structure directly from previous seismic events. The master templates, therefore, contain contributions from both direct and scattered seismic energy. We refer to this strategy as empirical MFP.

Empirical MFP breaks the signals into a large number of narrow frequency bands, chooses processing parameters that make signals in the narrow bands approximately independent, performs the matching operation band by band and combines the results incoherently across bands. The independence of the signal in the narrow bands helps to reduce the complication made by the source time history of the events [*Harris and Kvaerna*, 2010]. When performing the matching operation, we develop a steering vector calibration for the network of seismic stations in each narrow frequency band for each potential source location defined the master events. This vector of complex weight can be calculated as the principal eigenvector of the covariance matrix estimated from each master template.

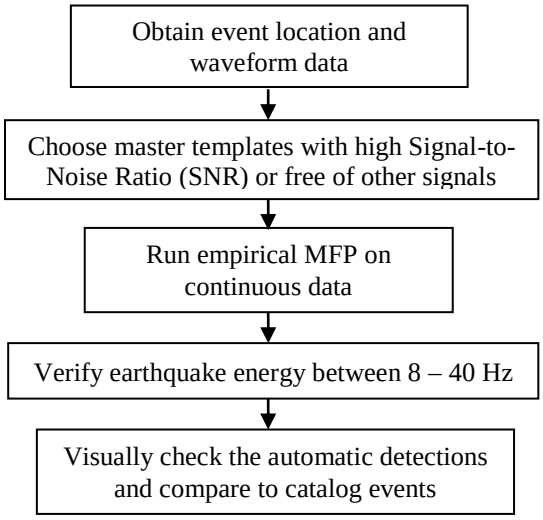

Figure 2. Empirical MFP work flow.

Our detection methodology can be described in 5 steps (Figure 2). The first step is to obtain the locations and waveforms of the catalog events. The second step is to determine which events should be chosen as field calibration events. Waveforms of calibration events must have high signal-to-noise ratios. The records must also be free of additional seismic events within a specified time window that

spans both before and after the actual microearthquake signal. Step 3 is to run the empirical MFP code on one day of continuous seismic data from all available seismic channels to identify events in the data stream that can match to the master templates. In the fourth step we verify that energy can be detected between 8 – 40 Hz to exclude matches between low-frequency noise in templates and continuous data. Finally, we visually verify all new detections and compare to catalog events.

Event Locations and Waveforms

For the event locations, we have both the original hypoinverse solutions from the SCEDC catalog and the waveform cross-correlation relocation results by *Hauksson et al*. [2012]. As the catalog of *Hauksson et al.* [2012] provides a better relative location of the events by performing the waveform cross-correlation, we plot all events using the locations from the Hauksson et al. [2012] catalog. There are 2977 catalog events by *Hauksson et al.* [2012] during January 2008 to December 2010 within a 10 km radius centered at seismic station HAT (Figure 1).

Continuous seismic data from the EN network was downloaded from the SCEDC website. The sample rate of the continuous data is 100 samples per second (SPS).

Master events selection

Theoretically, as more master templates are located throughout the study volume, we would be able to identify more new events. Therefore, we visually inspected the waveforms of all events between 2008 and 2010 that were in the original SCEDC catalog and identified those with the best quality data. These events have little noise, especially in the lower frequency ranges, and do not have significant seismic events within a 70 sec time window that includes the proposed master event. The master events must also include at least four stations with good quality recordings. We identify 231 master events out of the original 2977 catalog events (Figure 1).

In general, the background noise is incoherent across the 70 sec time window at stations ELM, ENG, HAT, OBS, RED, and YOU. However, station LIN displays a higher background noise level than the other stations. Therefore, we decided to remove station LIN from the processing due to its poor quality of recording. The other stations do not consistently display high background noise energy.

Run empirical MFP

The empirical MFP code performs its calculation on the continuous data using a 70-sec window which steps forward 1 second at a time. Figure 3 shows a 10-day example of results for the time period January 11th – 20th, 2010. This segment of data is band-pass filtered between 4 - 10 Hz. The y-value at each time point indicates the normalized detection statistic. A value of 1 would indicate an exact match between the template and the incoming seismicity at that particular time. Threshold levels for each detector are calculated over each 1-day period and are a function of the average detection statistic value. Detection statistics above the threshold are compared to detections at other detectors. If multiple detectors identify the same event, the detector with the largest detection statistic is then determined to have detected the event. The two detectors in Figure 3 show representative behavior.

As illustrated in Figure 3, Detector 157 (origin time: 2010/01/13, 14:14:30) shows an elevated detection statistic around January 15. Detector 157 is able to correctly identify itself with a detection statistic of 1 at the appropriate time. Detector 1 (origin time: 2008/01/21, 03:29:28) has a totally different detection pattern from Detector 157 and detected very few events. An investigation into the relative location of these detectors shows that Detector 157 is located in the middle of the January 15 earthquake swarm while Detector 1 is located on the fringe of the seismicity. This illustrates the fact that the more spatially evenly sampled the master events are, the higher chance we will have to be able to detect more events within the study volume.

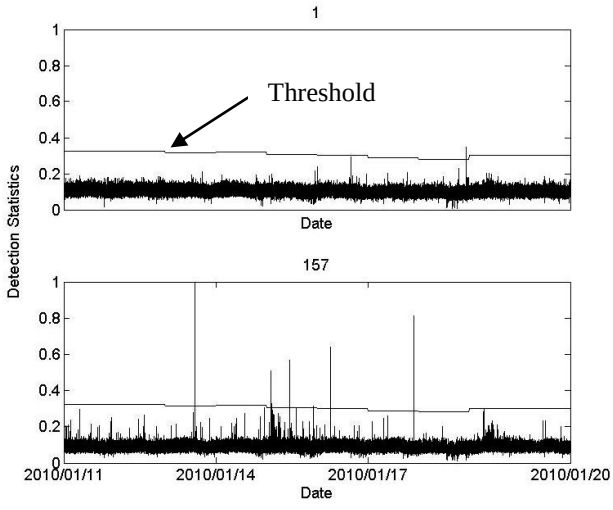

Figure 3. Empirical MFP detection results from two master templates during January 11th – 20th, 2010.

Spectrogram Check

The automatic spectrogram check identifies whether a proposed detection is a real event by checking the strength of the signals in the 8 – 40 Hz range. We calculate a function based on the ratio between the energy around the arrival time of the proposed event to the pre-event energy. If the function is above a certain threshold at over half of the channels, the proposed event is ruled to be real event. After a thorough study, we verified that this procedure delivers similar results to a manual inspection on the proposed detections.

Visual inspection and catalog check

The final step is to visually check the detections claimed by the spectrogram check and to exclude nearby regional events that fall outside our study area, but produced a signal across the local network. These nearby events are excluded by comparing the timing of the new events with the regional earthquake catalog.

MFP RESULTS AND DISCUSSION

For this study, we applied the empirical MFP method to continuous data collected between November 2009 and December 2010. We compared 231 master templates to the data stream and identified 6496 local events. The *Hauksson et al*. [2012] catalog reported 1536 events and the SCEDC catalog reported 1562 events over the same period (Figure 4). Therefore, we believe that our method demonstrates that MFP is a powerful tool to help identify more events than those identified using conventional event detection methods.

Figure 4 shows the impact of the nearby and extremely large 4 April 2010 Mw 7.2 El Mayor-Cucapah earthquake and aftershock sequence across our network. The fault rupture extended 75 km northwest, from the epicenter in Baja California through the US-Mexico border (http://www.scsn.org). More than 4000 aftershocks occurred afterwards, including 5 earthquakes greater than magnitude 6. Due to the close distance between the ruptured fault area and our study area, many aftershocks were recorded by the EN network. These events are easily excluded by comparing the potential detection list with the regional earthquake catalog.

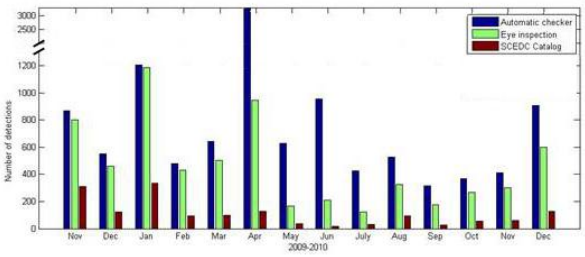

Figure 4. Final results of empirical MFP and comparison to the number of catalog events in the Hauksson et al. [2012].

We also reconcile the local catalog of events with our results. Our method found 306 of the 333 catalog events reported in the *Hauksson et al.* [2012] catalog during January 2010. There are 8.1% catalog events still missing. This is likely due to a lack of full coverage of the master templates of the seismogenic region (see Figure 1). Therefore, some events near the region where no master templates located might be missed in our empirical MFP method. However, with more and more data available as time goes on, we expect to have a full coverage over the whole region eventually.

Parameter optimization

We investigate three different frequency bands: 2 – 8 Hz, 4 – 10 Hz, and 6 – 12 Hz to determine the best frequency band on which to apply the empirical MFP method.

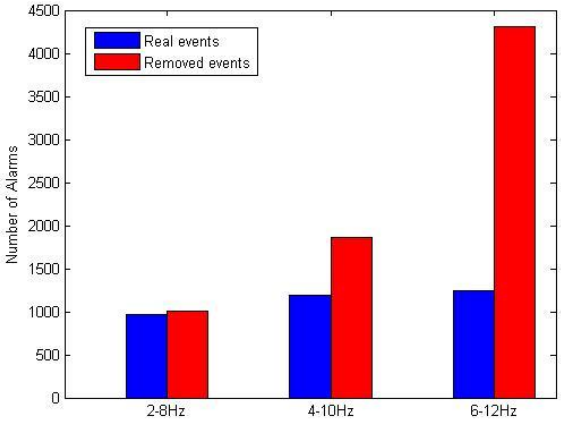

Figure 5. Number of real events and removed events found by the empirical MFP method within different frequency bands: 2-8 Hz, 4-10 Hz, and 6-12 Hz. The true events are in blue and false alarms are in red.

Figure 5 shows the comparison between the number of real events and the number of initial detections that were subsequently removed after the spectrogram check. It shows that more real events are identified at the higher frequency ranges, however the number of

potential detections that were ultimately removed increased significantly as well. The extra events identified at the higher frequency ranges tended to be weak events with the extra events in the 6 – 12 Hz range even weaker than the extra events in the 4 – 10 Hz range. Based on these results, we recommend the use of the 4 – 10 Hz frequency range during applications to larger datasets since this band detected a reasonable large number of events and balanced it with a reasonable number of events that were subsequently excluded in the processing.

The underlying issue is speed. The spectrogram check step is a relatively slow step compared to the computationally fast MFP step. The majority of the computation time is spent in verifying that there is energy in the 8 – 40 Hz range after initial identification of events from the MFP algorithm. We can further improve the efficiency by reducing the number of events that must go through this step. We believe that these initial detections are caused by a low-level match between the noise in the master event templates and the continuous seismicity.

Coulomb stress investigation

We calculate the static stress changes caused by the displacement of a fault using Coulomb3 [*Lin et al. 2004; Toda et al. 2005*]. Coulomb3 can calculate static displacements, strains, and stresses at any depth caused by fault slip, magmatic intrusion or dike expansion/contraction. We use the focal mechanism catalog of *Yang et al.* [2012] to get the geometry of the faults. The largest earthquake in our dataset is M3.78. We focus on 21 events with magnitude above 2. Then we calculate the Coulomb stress change due to those rupture faults and overlay the background seismicity between November 2009 and January 2010 in this region. We discovered that most of the earthquakes occurred in the increased Coulomb stress region.

Table 1 summarizes the 21 events with focal mechanism information which are used in our study. There are two major swarms within the EN network: the smaller one (swarm1) is close to station LIN and the larger one (swarm2) close to station ELM and HAT. Figures 6 and 7 show the Coulomb stress change in both map view and the cross section in the depth view for swarm 1 and swarm 2, respectively. The background seismicity is plotted on top of the Coulomb stress change maps. Although it is somewhat difficult to see in the cumulative snapshots in Figures 6 and 7, the majority of the seismicity occurred in the positive column stress change regions.

Table 1. Focal mechanism catalog information used in the Coulomb stress modeling by Yang et al. [2012]. The catalog format is in the order of: year, month, day, hour, minute and seconds, event ID, latitude and longitude, depth(km), magnitude, strike, dip, rake, fault plane uncertainty, number of P wave first motions, misfit of first motions, number of S/P amplitude ratios, average log_{10}(S/P amplitude ratio) misfit and quality of focal mechanism.

swarm 1																				
2009	11	1	10	23	12.94	10488245	33.151	-115.66	3.27	2.14	334	69	-151	32	27	28	0.25	25	0	B
2009	11	1	10	31	29.77	10488285	33.151	-115.66	3.27	2.15	342	80	-163	39	37	15	0.36	21	0	D
2009	11	1	19	28	36.15	10488485	33.1525	-115.642	2.79	2.35	358	76	157	24	24	33	0.17	28	1	A
2009	11	1	20	46	51.92	10488533	33.15217	-115.642	2.61	2.39	93	29	11	32	30	30	0.26	30	1	B
2009	11	1	21	23	52.38	10488549	33.152	-115.645	2.34	2.22	359	85	120	27	24	37	0.13	27	1	D
2010	1	23	13	16	16.26	10533437	33.14967	-115.644	3.37	2.57	336	43	-179	28	22	25	0.19	30	1	A
2010	1	23	13	17	16.55	10533445	33.15033	-115.643	3.99	3.03	167	82	-154	25	29	26	0.17	30	1	B
2010	1	23	13	33	55	10533565	33.151	-115.642	3.66	2.13	335	53	-173	24	26	32	0.1	20	1	A
2010	1	23	13	40	33.59	10533597	33.14983	-115.645	3.73	2.53	343	42	-151	27	34	40	0.09	26	1	B
swarm 2																				
2009	11	17	22	52	12.83	14545476	33.17067	-115.6	3.03	3.19	348	11	173	20	21	36	0.11	36	0	A
2009	11	17	23	5	36.41	14545540	33.17233	-115.603	3.34	3.31	352	76	176	42	28	22	0.16	37	0	B
2009	11	17	23	7	15.73	14545572	33.17383	-115.598	3.22	3.14	320	18	47	32	42	19	0.38	23	1	C
2009	11	18	0	43	59.99	14545820	33.17533	-115.601	3.65	3.36	161	84	89	31	27	34	0.29	38	0	B
2009	11	18	0	44	46.23	10141046	33.177	-115.597	3.12	2	337	60	-95	48	45	10	0.39	2	1	D
2009	11	18	10	34	26.61	14546284	33.16967	-115.604	3.78	2.67	144	76	-162	19	21	52	0.18	34	0	A
2010	1	15	2	1	34.07	10526869	33.17417	-115.599	3.91	3.05	322	88	142	27	39	15	0.14	32	0	B
2010	1	15	2	3	14.54	10526893	33.17484	-115.594	4.39	2.25	318	77	-153	41	37	14	0.11	2	2	C
2010	1	15	2	12	56.49	10526957	33.17633	-115.597	3.78	3.42	163	76	-123	32	35	29	0.03	38	0	D
2010	1	15	2	13	51.71	10526965	33.1725	-115.599	3.9	3.52	162	86	-124	21	26	20	0.21	15	1	A
2010	1	15	11	27	48.1	10528285	33.17817	-115.601	4.45	2.04	201	76	-96	23	22	23	0.24	25	1	A
2010	1	15	20	47	26.26	10529109	33.177	-115.597	3.72	2.03	334	90	159	24	27	20	0.16	20	1	B

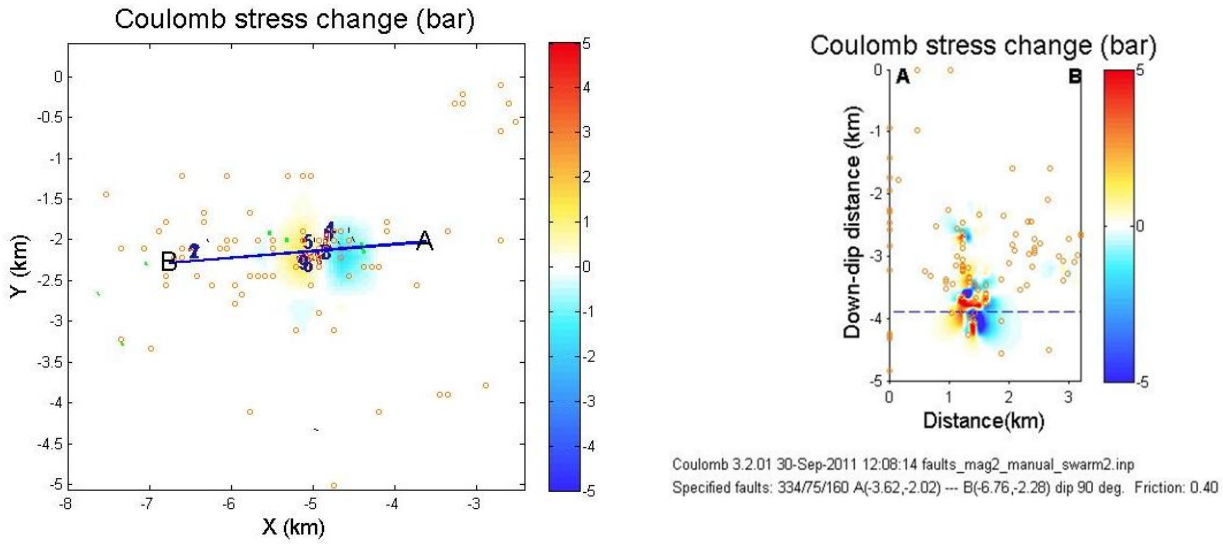

(a) (b)

Figure 6. (a) Coulomb stress change of swarm 1 (close to station LIN) in the map view. (b) Coulomb stress change of swarm 1 in the cross section A-B. The background seismicity (orange dots) is overlay on each plot. Each fault plane projected to the surface is identified by the number.

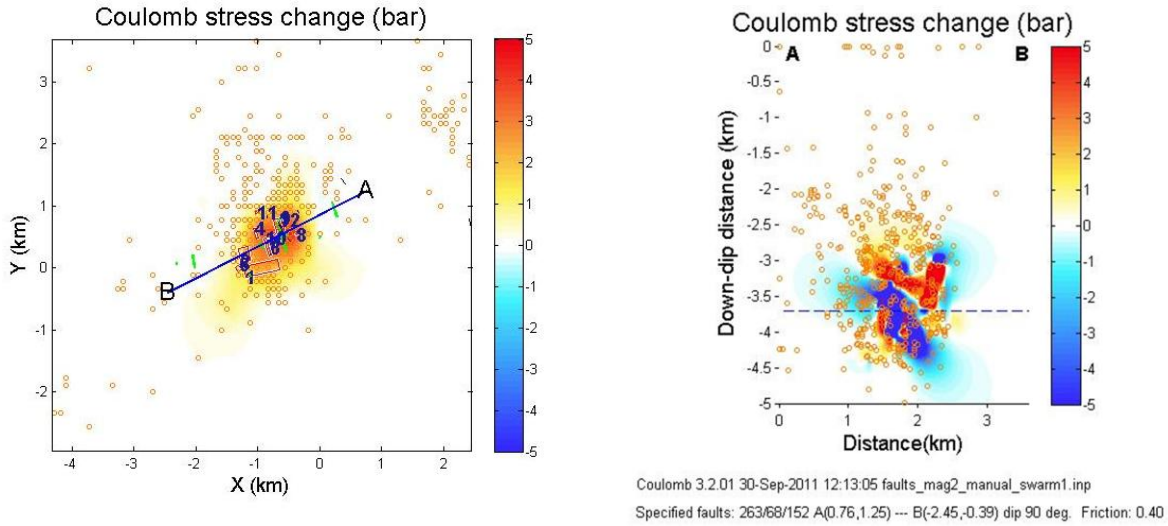

(a) (b)

Figure 7. (a) Coulomb stress change of swarm 2 (close to station ELM and HAT) in the map view. (b) Coulomb stress change of swarm 2 in the cross section A-B. The background seismicity (orange dots) is overlay on each plot. Each fault plane projected to the surface is identified by the number.

Magnitude of the new events

We also investigate the magnitude of the new events in our study. Firstly, we define the SNR of the signal using

$$SNR = \frac{\text{Amplitude of signal} - \text{Amplitude of noise}}{\text{Amplitude of noise}}$$

We obtain the amplitude of the signal by stacking the P wave energy over all available vertical components. We determine the amplitude of noise by averaging the absolute value over 2-second window right before the event origin time. In Figure 8, a regression line was drawn to obtain the empirical relationship in our region between the magnitude and $\log_{10}$ (SNR) of the catalog events. The newly detected events not reported by the *Hauksson et al.* [2012] catalog, are plotted along the regression line

to obtain an estimated magnitude based on the above empirical relationship.

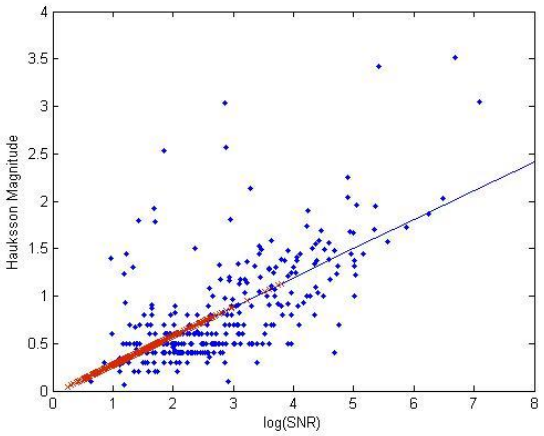

Figure 8. Regression relationship between the magnitude and log_{10}(SNR). The blue dots are the catalog events. The new events are plotted in red along the regression line.

A histogram of events detected by both the *Hauksson et al.* [2012] catalog and the MFP method is plotted in Figure 9. The new events detected only by the MFP method are plotted in red and the catalog events are in blue. It is clear that the MFP method greatly increases the catalog completeness of the smaller magnitude events.

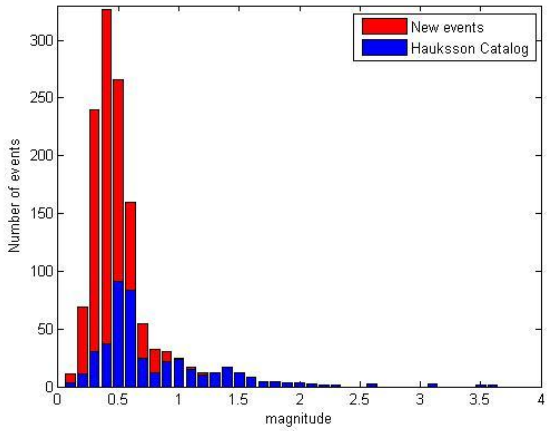

Figure 9. Histogram of the number of events versus the magnitude of the events. The red bars are events detected by the MFP method only. The blue bars are events detected by both MFP and the catalog.

CONCLUSIONS

MFP with empirically calibrated master templates is able to detect more events than can be detected using only conventional techniques. Unlike most array processing methods, empirical MFP does not require a plane wave assumption. Therefore, empirical MFP is more flexible in noisy environments, as long as the master templates adequately cover the area where future events will possibly occur. Our test on SSGF continuous data between November 2009 and December 2010 demonstrates the detection capability using the empirical MFP method. There are 6496 local events detected in total by the MFP method within the 4 – 10 Hz frequency band, while the catalog reports only 1536 events. Thus the empirical MFP algorithm significantly improves seismic array detection capability. A higher frequency band tends to find more weak events but is accompanied with a greater number of events that were subsequently removed during the spectrogram check step. We balanced the number of real events and the number of removed detections by selecting 4-10 Hz and as the optimal parameters in this case study. In addition, we investigated the Coulomb stress changes in the region beneath the EN network during a time period when two major earthquake swarms occurred. We verified that the majority of the microseismic events occurred in the positive Coulomb stress region, which is consistent with the stress regime of the rupture faults. Finally, we estimate the magnitude of the new events identified by the MFP method. The result shows that most of the new events are low amplitude events with magnitudes between 0 and 1, which clearly demonstrates the improvement of the MFP method on the detection capability of the network for the local earthquakes.

ACKNOWLEDGEMENTS

This work was performed under the auspices of the U.S. Department of Energy by Lawrence Livermore National Laboratory under contract ED-AC52-07NA27344. This work is funded by the American Recovery and Reinvestment Act, Pub. L. 111-5. We thank Robert Mellors, William Walter and Sean Ford for their helpful discussions and comments to improve this manuscript.

REFERENCES

Allis R., J.N. Moore, J. McCulloch, S. Petty, and T. DeRocher, (2000). "Karaha-Telaga Bodas, Indonesia: A Partially Vapor Dominated Geothermal System." Geothermal Resources Council *Transactions*, v. 24, p. 217-222.

Baggeroer, A. B., Kuperman,W. A. and Mikhalevsky, P.N., (1993). An overview of matched field methods in ocean acoustics, *IEEE Journal of Oceanic Engineering*, 18(4), 401–424.

Bucker, H. P., (1976). Use of calculated sound fields and matched field detection to locate sound

sources in shallow water, *Journal of the Acoustical Society of America*, 59(2), 368–373.

Fuis, G. S., W. D. Mooney, J. H. Healy, G. A. McMechan, and W. J. Lutter, (1984), A seismic refraction survey of the Imperial Valley region, California, *Journal of Geophysical Research*, 89, 1165-1189.

Fuis, G.S., and Mooney, W.D., (1990), Lithospheric structure of California along the San Andreas fault system, from seismic and other data, in Wallace, R.E., edit., the San Andreas fault system: USGS Prof. Paper 1515, 207-236.

Gibbons, J. S., M. B. Sørensen, D. B. Harris, and F. Ringdal. (2007), The detection and location of low magnitude earthquakes in northern Norway using multi-channel waveform correlation at regional distances, *Physics of The Earth and Planetary Interiors*, **v. 160**, no. 3-4, 285-309.

Hooland, A. A. (2002), Microearthquake Study of the Salton Sea Geothermal Field, California: Evidence of stress triggering. Idaho National Engineering and Environmental Laboratory, Geosciences Department. *Thesis*, The University of Texas at El Paso.

Harris, B. D., and T. Kvaerna, (2010), Superresolution with seismic arrays using empirical matched field processing, *Geophysical Journal International*, **182**, 1455-1477.

Hauksson, E. and W. Yang, and P.M. Shearer, Waveform Relocated Earthquake Catalog for Southern California (1981 to 2011). (2008), In submission: *Bulletin Seismological Society of America*,

Kohler, M., H. Magistrale, and R. Clayton. (2003), Mantle heterogeneities and the SCEC three-dimensional seismic velocity model version 3, *Bulletin Seismological Society of America*, **93**, 757-774.

Lin, J. and R.S. Stein (2004), Stress triggering in thrust and subduction earthquakes, and stress interaction between the southern San Andreas and nearby thrust and strike-slip faults, Journal of Geophysical Research., 109, B02303, doi:10.1029/2003JB002607.

Magistrale, H., S. Day, R. W. Clayton, and R. Graves. (2000), The SCEC southern California reference 3D seismic velocity model Version 2, *Bulletin Seismological Society of America*, **v. 90**, no. 6B, S65-S76.

Peng, Z., and P. Zhao. (2009), Migration of the Parkfield early aftershock sequence, *Nature Geoscience*, doi: 10.1038/ngeo697.

Shelly, D. R., G. C. Beroza, S. Ide, and S. Nakamula (2006), Low-frequency earthquakes in Shikoku, Japan and their relationship to episodic tremor and slip, *Nature*, 442, 188-191.

Toda, S., R. S. Stein, K. Richards-Dinger and S. Bozkurt (2005), Forecasting the evolution of seismicity in southern California: Animations built on earthquake stress transfer, *Journal of Geophysical Research*, B05S16, doi:10.1029/2004JB003415.

Waldhauser, F. (2001), "hypoDD -- A program to compute double-difference hypocenter locations," *U.S. Geological Survey Open-File Report*, 01-113.

Waldhauser, F., and William L. E. (2000), A double-difference earthquake location algorithm: Method and application to the northern Hayward fault, California, *Bulletin Seismological Society of America*, **90**, 1353-1368.

Yang, W., E. Hauksson and P. M. Shearer, Computing a large refined catalog of focal mechanisms for southern California (1981 - 2010), manuscript in preparation, 2012.